Fast-ion-beam laser-induced-fluorescence measurements of branching fractions and oscillator strengths in Nd II

R. Li, S.J. Rehse, T.J. Scholl, A. Sharikova, R. Chatelain, R.A. Holt, and S.D. Rosner

Abstract: We measured the spontaneous-emission branching fractions of 46 levels in Nd II, selectively populated via single-frequency laser excitation of a 10 keV ion beam. The levels studied had term energies up to 29 955 cm^{-1}, and decay branches with spontaneous emission in the range 372–850 nm were detected. The experimental accuracy for branching fractions over 0.1 was ~7%. We used these branching fractions along with our previously determined radiative lifetimes to infer transition probabilities and oscillator strengths for 430 transitions, which are useful for stellar abundance determinations.

PACS Nos.: 32.70Cs, 95.30Ky

Résumé : Nous avons mesuré les rapports de branchement d'émission spontanée de 46 niveaux du Nd II peuplés sélectivement via l'excitation laser monochromatique d'un faisceau d'ions de 10 keV. Les niveaux étudiés ont des termes d'énergie jusqu'à 29 995 cm^{-1} et nous avons observé des branches de désexcitation spontanée dans le domaine 372–850 nm. La précision expérimentale pour les rapports de branchement au delà de 0.1 était ~7 %. Nous avons utilisé ces rapports de branchement avec les temps de vie radiatifs déjà déterminés pour en déduire les probabilités de transition et les forces d'oscillateur pour 430 transitions qui sont utiles dans l'étude des abondances stellaires.

[Traduit par la Rédaction]

1. Introduction

A knowledge of the atomic properties of the lanthanide ions is vital to astrophysical studies of chemically peculiar (CP) stars of the upper main sequence, metal-deficient stars of the galactic halo, and the Sun [1, 2]. Measurement of the abundances of these heavy elements in the photospheres of these stars can lead to a better understanding of their original nucleosynthesis and the radiative, convective, and gravitational processes that determine their preferential migration from the core to the surface. The lanthanide elements provide an opportune test case for such astrophysical studies in that they form a contiguous sequence of atomic numbers. This continuity allows astrophysicists to study the odd–even abundance variation resulting from the nuclear-pairing interaction. More importantly, the lanthanides

Received 11 September 2006. Accepted 2 May 2007. Published on the NRC Research Press Web site at http://cjp.nrc.ca/ on 21 November 2007.

R. Li, S.J. Rehse, T.J. Scholl, A. Sharikova, R. Chatelain, R.A. Holt, and S.D. Rosner.[1] Department of Physics & Astronomy, University of Western Ontario, London, ON N6A 3K7, Canada.

[1]Corresponding author (e-mail: rosner@uwo.ca).

 doi: 10.1139/P07-077

present numerous examples of isotopes that may be formed by the r-process, the s-process, the p-process, or a combination. In comparison to solar abundances, the lanthanides are present in CP stars in great excess; for example, in Przybylski's star (HD 101065), the excess abundance of rare earth elements is 3–4 dex [3]. In CP stars with measurable magnetic-field effects, the spectral lines of the lanthanide elements are among the most enhanced [2]. Several galactic halo stars have recently been discovered with extremely large relative lanthanide abundances. These stars are among the oldest stars in our galaxy, and have the potential to provide much information about nucleosynthesis in novae and supernovae. Lastly, the study of lanthanides in the solar spectrum is experiencing a resurgence of interest with the availability of satellite spectra in the UV and laboratory data from new techniques. Some of the reasons for this interest are the potential contribution of two free electrons by the lanthanides to the solar opacity, the realization that diffusion, which has had a significant fractionating effect on helium [4], may well have affected the heavier elements in the Sun, and increasing caution with regard to the accuracy of meteoritic abundances. Beyond astrophysics, the atomic properties of the lanthanides are needed in the design of commercial high-intensity discharge lamps [5] and in the use of spectra to probe the crystalline structure of divalent and trivalent crystal salts [2].

Nd in particular is one of the most abundant rare-earth elements. Overabundance of Nd has been found and studied in many CP stars, for example, the HgMn star HR 7775 [6], the Ap star HD 24712 [7], and the Am star β Aur [8]. As a stable nuclear species, Nd is also useful for estimating the age of the Galactic halo [9]. The Th:Nd abundance ratio in G-dwarf stars was investigated to determine the age of the Galaxy [10]. Recently, astrophysicists have been using Nd spectra to study abundance stratification and pulsation in rapidly oscillating Ap stars [11].

The key atomic data required for the determination of elemental abundances from observed spectra are oscillator strengths, f. For many years, the main source of these data for many elements were the NBS monographs, with values based on absolute intensity measurements and calculated atomic densities [12, 13]. In this work, the factors of error in absolute values of gf ($g = 2J + 1$), ranged from 1.7 to 2.0 as the upper-level term energy varied from 1.5×10^4 cm^{-1} to 5.0×10^4 cm^{-1}. In the case of Nd II, as with many of the lanthanides, the scarcity of coverage of its very rich spectrum and the large uncertainties seriously limited the accuracy of derived abundances.

A better approach to determining oscillator strengths is to combine data on the branching fractions (BFs) for all transitions from a given level with the measured spontaneous emission lifetime of that level. Maier and Whaling [14] measured BFs in a hollow-cathode discharge and incorporated the beam-foil lifetime measurements of Andersen et al. [15] to obtain transition probabilities for transitions from 9 levels of Nd II. Ward et al. [16] measured radiative lifetimes for 8 levels of Nd II and used them to correct old gf-values deduced from the NBS arc-spectra measurements. Kurucz [17] compiled experimental transition probabilities in a form that is available online [18], using the data of Maier and Whaling, BFs from the intensity measurements of Meggers et al., together with experimental lifetime data.

Quite recently, two determinations of oscillator strengths have been made utilizing radiative lifetime measurements obtained by laser-induced-fluorescence (LIF) measurements. Xu et al. [19] performed relativistic Hartree–Fock (HFR) calculations of BFs for 24 levels and combined them with their own time-resolved LIF lifetime measurements to calculate oscillator strengths for 107 transitions; these are available online from the DREAM database [20]. The estimated uncertainties in the oscillator strength determinations were assigned as "$\leq$10% for the strongest transitions."

Den Hartog et al. [21] determined transition probabilities and oscillator strengths for over 700 transitions by combining their own time-resolved LIF lifetime measurements for 168 levels with BF measurements obtained using Fourier-transform spectrometry (FTS) of emission from an Ar–Nd hollow-cathode discharge lamp. Their uncertainties are typically $\sim$10%, less for strong transitions and greater for weak ones.

Prior to the work of both Xu et al. and Den Hartog et al., our own group at the University of Western Ontario (UWO) measured the spontaneous-emission lifetimes of 48 levels in Nd II with fast-ion-beam

LIF techniques [22, 23]. We have also recently determined the hyperfine structure and isotope shifts in 110 transitions in Nd II utilizing the collinear fast-ion-beam/laser method (FIBLAS) [24]. A comparison of the UWO and the Xu et al. lifetimes showed agreement within experimental error (a few percent in both cases), although there was a hint of a systematic divergence for lifetimes longer than 60 ns. A comparison of the UWO and the Den Hartog et al. lifetimes showed agreement within error (±5% for both sets of data) for 47 energy levels. Of these, no lifetimes exhibited a disagreement exceeding 10%, with one exception: the lifetime measurements for the energy level 29 260.740 cm^{-1} differed by a factor of two. As a result of the high selectivity of the current measurements, we have determined that this level was misidentified in ref. 23 due to an error in the database of ref. 17 and is actually 28 285.619 cm^{-1}, removing the disagreement.

The current work describes the measurement of branching fractions for 46 levels in Nd II using LIF in a collinear beam-laser apparatus. We present the first experimental determination of Nd II transition probabilities obtained from lifetime and branching fraction measurements performed in the same beam-laser apparatus. This method has the advantage of being remarkably free of systematic errors arising from spectral blending and misidentification of transitions.

2. Experimental method

Among techniques for the experimental determination of branching fractions, the "beam-laser" method, first demonstrated in ref. 25, is one of the most reliable. This spectroscopic technique involves selective excitation of a single state in a single-species ion beam followed by direct observation of the subsequent LIF. All decay branches originating from this selectively populated state with a transition wavelength within the spectral viewing range are observed and can be assigned with absolute certainty to that excited state. The signal-to-noise ratio (SNR) provided by laser excitation is excellent for typical conditions of integration times of ∼1 s or greater and ion currents of ∼100 nA or greater. Furthermore, excellent suppression of background light can be achieved using Doppler-modulation of the laser frequency (see below).

Our experimental apparatus, which has been described in detail elsewhere [25], is shown in Fig. 1. Nd^+ ions were produced in a modified Danfysik 911A source without an arc discharge; ionization occurred on the surface of a hot tungsten filament. Under such conditions, we observed stable beams of Nd^+ ions produced in metastable levels up to ∼6000 cm^{-1}. Ion beam currents of ∼100 nA were typical and the actual current as detected by a secondary-electron-suppressed Faraday cup was monitored by a data acquisition computer. After acceleration to 10 keV, the ions were focused, mass-filtered by a Wien velocity filter, and then electrostatically deflected to overlap a counter-propagating laser beam.

The single-frequency laser beam used for excitation was produced by an argon-ion-pumped Coherent 699-21 dye laser running with Stilbene-3 dye. Stilbene-3 has a nominal tuning curve from 415–465 nm, so only Nd II levels that could be excited via transitions within this wavelength range were studied. The laser wavelength was determined to ∼1 part in 10^7 by a traveling Michelson interferometer with a polarization-stabilized reference helium–neon laser [26, 27]. In the region of laser excitation and fluorescence, the laser beam was softly focused to a 0.5 mm-radius waist by a 2 m focal-length lens; the typical laser power in this region varied from 150 to 35 mW, depending on the dye gain. With the wavelength meter, the laser wavelength was set to correspond to any desired "pump" transition (a transition used to excite the ion from a ground or metastable state to the energy level of interest). Typically, this was the transition within the dye tuning range with the largest transition probability. Ion resonance with the antiparallel propagating laser beam was confined to a small region with a high degree of optical access (the "post-acceleration" region) by a modification of the "Doppler-switching" technique [28]. As the ions entered this region, they were accelerated by a DC potential difference of approximately −500 V and brought into resonance with the Doppler-shifted laser beam. To suppress background light from the laser and ion collisions with background gas, a sinusoidal voltage of ∼20 V peak-to-peak at 2 kHz was added to the DC potential. The resulting modulation of the laser frequency

Fig. 1. Apparatus for branching-fraction measurements. A Nd^+ ion beam of ~100 nA is overlapped with a collinear antiparallel single-frequency cw laser beam tuned to excite a Doppler-shifted energy level in a post-acceleration region whose potential is modulated at 2 kHz. Fluorescence from all the decay branches is collected with arrays of optical fibers, spectrally analyzed in a Czerny–Turner monochromator, and detected by a photomultiplier connected to a lock-in amplifier. A second identical monochromator set to the wavelength of one of the decay branches provides a normalization signal. A data acquisition computer controls wavelength scanning of the monochromator and records the LIF intensity as a function of wavelength, as well as the ion current, laser power, and the output of the normalization channel. A third lock-in amplifier is used to stabilize the dye laser frequency against wavelength and Doppler-shift drift.

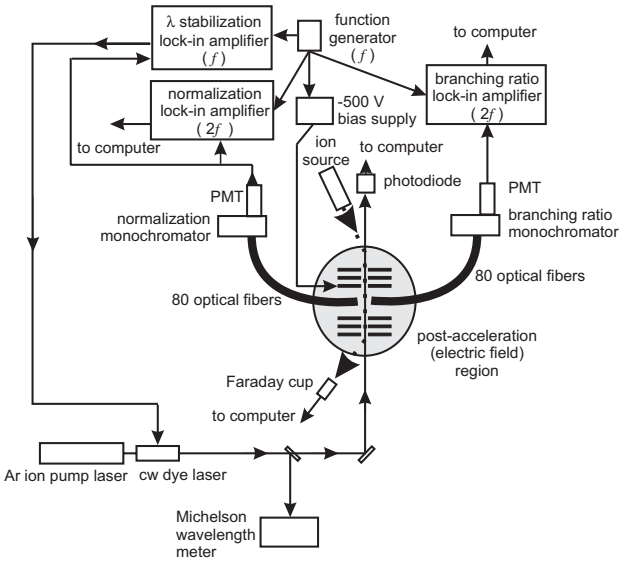

in the ion rest frame allowed subsequent lock-in detection of the LIF signals. The signals from the more intense lines were easily measurable as DC signals on an electrometer (~10 nA), but lock-in detection was used both to suppress the background signal and to provide a derivative-shaped signal to stabilize the laser frequency to the atomic resonance.

The spontaneous-emission LIF from the resonant ions was collected by two arrays of polyimide-coated quartz/quartz optical fibers whose ends were arranged in circles in alternating planes perpendicular to the ion beam and (or) laser beam axis. The LIF from one array was used for branching-fraction data while the other provided a "normalization" signal that was used to correct the branching-fraction signal for variations in the excitation rate due to drifts in intensities and overlap of the laser and ion beams. Because the excitation of the ions is anisotropic and the LIF is not collected from a 4π solid angle, a measured intensity ratio for two branches (corrected for detector efficiency) can differ from its true value, which is defined for isotropic excitation and (or) detection. To this end, the angular distribution of the fiber ends from the two fiber arrays in each plane was deliberately chosen to be non-uniform. With the direction of the electric field of the vertically polarized laser defined as $\theta = 0$, the fibers of one array (typically used to record the normalization signal) were placed at or near the "magic" angle, $\theta_{\text{magic}} = \cos^{-1}\left(1/\sqrt{3}\right) \approx 54.7°$, where the angular distribution of fluorescence from $\Delta M = \pm 1$ transitions has the same intensity as that for $\Delta M = 0$ transitions. The fibers of the second array (typically used to record the branching fraction signal) were distributed around the circle with a density $\mathrm{d}N/\mathrm{d}\theta$ weighted as $\sin\theta$. This spacing ensured that the ratio of detected fluorescence from any two branches was identical to its value in the case of isotropic excitation or detection. A detailed analysis is given in the Appendix of ref. 25.

Fig. 2. Branching-fraction spectrum from the energy level at 23 397.365 cm^{-1}, excited by pumping the transition at 436.86 nm from the 513.33-cm^{-1} metastable state. The LIF from the decay branches in the wavelength range 415–740 nm was recorded by scanning the monochromator in steps of 1 nm with a dwell time of 2 s per step, utilizing the 2400 groove/mm grating. The continuous line is a fit to the data of a model used to determine the relative line intensities. LIF from the transition at 427.27 nm was recorded as the normalization signal. The Nd^+ ion-beam current was 180 nA and the laser power seen by the ions was ~160 mW.

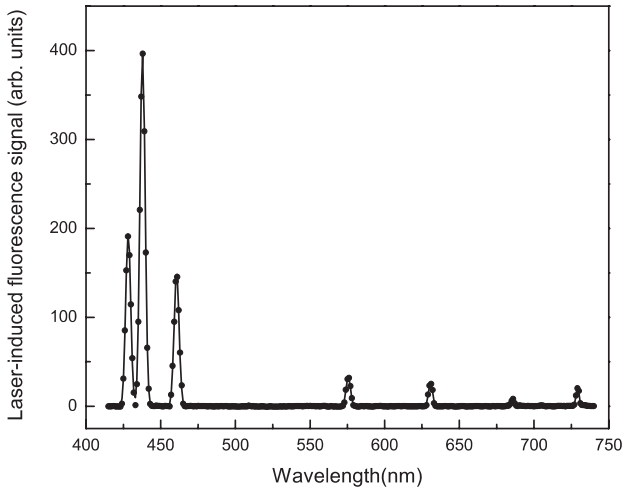

Each 80 fiber bundle terminated in a rigid coupling to the input slit of a 0.275 m, $f/3.8$ scanning monochromator (Acton Research Spectra-Pro 275). The 20 mm high slits were normally opened to their maximum width of 3 mm. Each monochromator had three gratings on a rotating carousel to provide complete spectral coverage. The first grating provided coverage from 250–500 nm, the second from 250–750 nm, and the third from 250–1500 nm. In cases where closely spaced emission lines precluded the resolution of individual lines, the entrance and exit slits of the monochromator were narrowed until the individual lines were resolved and the entire spectrum was obtained at that slit width. For the measurement of branches with wavelengths longer than 600 nm, a long-wavelength-pass filter (50% transmission point at 475 nm) was inserted to avoid observation of second-order diffraction from the grating.

The "normalization" monochromator was coupled to a bialkali-photocathode photomultiplier tube (PMT), ETL model 9235QB. During data acquisition this monochromator was set to the wavelength of the "normalization transition" — typically the transition with the largest anticipated transition probability not being used as the pump transition. Output from this PMT was analyzed by two lock-in amplifiers: one operating in "2f" mode for background suppression and one operating in "1f" mode for dye-laser wavelength stabilization.

With the laser wavelength locked to the peak of the pump-transition resonance, the "branching fraction" monochromator (Fig. 1), coupled to a thermoelectrically-cooled trialkali PMT (ETL model 9658R), was scanned to record the LIF spectrum from the lowest possible wavelength to ~850 nm. This signal was input to a third lock-in amplifier operating in $2f$ mode and its background-suppressed output was recorded on the data acquisition computer, which also controlled the scanning of the monochromator grating. A typical scan would step the monochromator grating 1 nm per step and would dwell for 2 s per step, taking from 5 to 15 min per scan. An example of a branching-fraction spectrum with excellent SNR is shown in Fig. 2.

3. Data and analysis

Branching fractions are obtained from a spectrum such as that shown in Fig. 2 by determining the relative intensities of all observed transitions from an excited stated. For transitions from an upper state (u) to a set of lower states (l), the relative intensities I_{ul} are obtained by dividing the areas S_{ul} of the observed spectral lines by the wavelength-dependent ratio of the measured response of our fiber/monochromator/PMT system, $r\ (\lambda_{ul})$, to the value of the manufacturer's spectral irradiance data for our lamp at that wavelength, $i\ (\lambda_{ul})$,

$$I_{ul} = \frac{S_{ul}}{[r\ (\lambda_{ul})\ /\ i\ (\lambda_{ul})]} \tag{1}$$

Branching fractions R_{ul} are then obtained as

$$R_{ul} = \frac{I_{ul}\lambda_{ul}}{\sum\limits_{l} I_{ul}\lambda_{ul}} \tag{2}$$

in which the λ_{ul} factors are needed to convert relative intensities into relative photon emission rates.

Obtaining accurate branching fractions from relative intensities assumes that all radiative transitions that contribute to the decay of the level have been observed. In practice, some weak branches (which must exist based on selection rules) fall below our threshold of detection, especially in the region beyond 850 nm where our detector response is negligible. To estimate the effect of these missing branches, it is useful to compare with the data of others. Maier and Whaling [14], who report no branching fractions for transitions with wavelengths greater than 636.6 nm, list four lines that are missing in spectra that we recorded. Three of these were also not listed by Den Hartog et al. [21], and the one that was is assigned a branching fraction of "<0.5%" in ref. 14. Den Hartog et al. list 10 lines that are missing or tentative in our spectra, with branching fractions <2%. Since the effect of such weak branches on the other branching fractions is smaller than the experimental uncertainties, we have not attempted to modify our branching fractions using these older data. Instead, in tabulating the relative intensities (see Table 2), we have included data for all transitions not seen by us but listed in the older data. These data give the reader an opportunity to gauge the effect of unobserved branches and to recalculate branching fractions from the relative intensities for relatively unambiguous cases. Because of the highly selective excitation in the present work and the resulting simple spectra, it is possible that some of these "missing" branches are incorrectly attributed in the older data, and are not actually missing.

The procedure for determining the areas under the emission peaks is been discussed in detail in ref. 25. A nonlinear least-squares fitting routine was used to fit a spectrum with Gaussian lineshapes, using as parameters a constant background, peak centres, peak areas, and a peak-width function that depended quadratically on wavelength. This choice was both robust and completely adequate to describe the nonlinear wavelength dependence of the linewidth inherent in the Czerny–Turner monochromator.

Typical statistical uncertainties in the fitted areas ranged from ∼0.2% to ∼27%, depending mainly on the peak size. When it was necessary to use more than one grating to record the complete set of branching fractions, the adjacent spectra were "merged" with a least-squares procedure that used the peaks appearing in both spectra .

The relative efficiency of our detector system (fiber array, monochromator, and PMT) varied smoothly as a function of wavelength. To compensate for this varying efficiency, the detector system response was calibrated with a 200 W NIST-traceable quartz–tungsten–halogen (QTH) lamp. Uncertainties in the calibration of the relative lamp emission due to manufacturer calibration and transfer from NIST standards as well as ageing of the lamp total 3.9%. This appears in Table 1 as "total lamp calibration".

Table 1. Estimated uncertainties in the determination of relative intensities.

Source of uncertainty	Uncertainty (%)
Systematic:	
Total lamp calibration[a]	3.9
Detector calibration procedure[b]	3.2
Statistical:	
Fit of line profiles to data[c]	∼0.2–5
Detector calibration procedure[d]	1.5

[a]NIST, transfer to Oriel lamp, lamp aging.
[b]Includes 0.2% for fiber attenuation effect.
[c]The range shown is from a sample of 6 spectra, and represents 70% of the distribution.
[d]The uncertainty shown is a sample mean.

Table 2. Relative intensities of branches from a given upper level. The intensities of branches that were too weak to analyze are indicated by "w". For transitions observed by others but not in this work, relative intensities were calculated from their data and included in the table. These entries are in italics.

Upper level energy (cm^{-1})	Lower level energy (cm^{-1})	Wavelength in air (nm)	Relative intensity
22696.885	513.322	450.658[a]	0.56(6)
	1470.097	470.972	0.55(6)
	1650.199	475.002	0.039(4)
	2585.453	497.092	0.17(2)
	3066.750	509.279	1
	4437.558	547.514	0.017(3)
	5487.657	580.923	0.084(9)
	6005.271	598.938	w
	6931.800	634.139	0.052(6)
	8420.321	700.257	0.032(7)
	9357.906	749.478	0.020(6)
	9877.173	779.835	0.08(2)
	10337.097	808.854	0.026(9)
	10942.012	850.478	0.07(3)
22850.552	0.000	437.503[a]	0.9(1)
	513.322	447.558	0.22(2)
	1650.199	471.559	1
	6005.271	593.474	0.12(1)
	7524.740	652.314	0.16(2)
	8420.321	692.799	0.08(1)
	8796.378	711.336	0.009(2)
	9198.395	732.284	0.025(4)
	9674.844	758.764	0.08(1)
	9908.650	772.472	0.037(7)
	10666.777	820.539	0.10(2)
	10887.246	835.660	0.08(1)
23159.979	513.322	441.443[a]	0.12(2)
	1470.097	460.916	0.026(8)
	1650.199	464.775	0.08(1)
	2585.453	485.903	1
	4512.481	536.117	0.08(2)

Table 2. (*continued*).

Upper level energy (cm^{-1})	Lower level energy (cm^{-1})	Wavelength in air (nm)	Relative intensity
	9357.906	724.330	w
	9887.165	752.646	0.019(6)
	10337.097	779.642	0.021(7)
	10883.260	814.326[b]	0.08(2)
	10941.995	818.241[b]	
23229.991	0.000	430.357[a]	1
	513.322	440.082	0.15(2)
	1650.199	463.267	0.022(3)
	3066.750	495.814	0.028(3)
	4437.558	531.982	0.26(3)
	6005.271	580.400	0.070(7)
	6931.800	613.396	0.006(1)
	7524.740	636.554	0.016(2)
23397.385	0.000	427.278	0.50(5)
	513.322	436.863[a]	1
	1650.199	459.701	0.39(4)
	6005.271	574.814	0.13(1)
	7524.740	629.841	0.14(3)
23397.385	8796.378	684.696	0.08(1)
	9198.395	704.083	0.022(3)
	9674.844	728.528	0.08(2)
	9908.650	741.156	0.018(2)
	10883.260	798.878[b]	0.016(3)
	10887.246	799.133[b]	
23409.537	0.000	427.057	0.41(4)
	513.322	436.632	0.35(4)
	1470.097	455.673[a]	0.32(3)
	1650.199	459.445	0.30(3)
	3066.750	491.438	1
	4437.558	526.947	0.19(2)
	6005.271	574.413	0.08(1)
	6931.800	606.713	0.034(5)
	7524.740	629.360	0.017(2)
	8420.321	666.963	0.037(5)
	9198.395	703.481[b]	0.014(2)
	9357.906	711.467[b]	
	9877.173	738.767[b]	0.017(3)
	9908.650	740.489[b]	
	10666.777	784.545[b]	0.039(6)
	10786.783	787.854[b]	
	10887.246	798.103	0.015(3)
23537.387	0.000	424.737[a]	1
	513.322	434.206	0.11(1)
	1470.097	453.033	0.035(4)
	1650.199	456.761	0.074(8)
	3066.750	488.369	0.027(3)
	4437.558	523.419	0.28(3)
	6005.271	570.224	0.11(1)
	7524.740	624.334	0.034(5)

Table 2. (*continued*).

Upper level energy (cm^{-1})	Lower level energy (cm^{-1})	Wavelength in air (nm)	Relative intensity
	9198.395	697.207	0.009(2)
	9877.173	731.852[b]	0.007(2)
	9908.650	733.542[b]	
	10883.260	*790.040*[c]	*0.004(1)*
	11709.600	845.236	0.08(2)
23857.278	513.322	428.257[a]	0.40(4)
	1470.097	446.560	0.46(5)
	1650.199	450.181	1
	4512.481	516.792	0.28(3)
	5487.657	544.226	0.38(4)
	6931.800	590.662	0.20(2)
	8420.321	647.618	0.06(1)
	9877.173	715.106	0.033(8)
24053.354	0.000	415.626	0.74(8)
	513.322	424.689	0.15(2)
	1470.097	442.682	0.15(2)
	1650.199	446.241[a]	1
	3066.750	476.362	0.34(4)
	4437.558	509.652	0.28(4)
	6005.271	553.922	0.08(1)
	6931.800	583.898	0.022(9)
	7527.740	604.845	0.016(8)
	8420.321	639.495	0.03(1)
	9877.173	705.214	0.04(1)
	10667.120	746.813[b]	0.019(9)
	10786.783	749.810[b]	
	10942.012	762.489	0.018(7)
	11709.600	809.906	0.03(1)
	12013.230	830.889[b]	0.02(1)
	12091.170	835.459[b]	
	12222.185	844.994[b]	
	12232.706	845.745[b]	0.03(1)
	12276.210	848.871[b]	
24134.095	513.322	423.237[a]	0.80(8)
	1470.097	441.105	0.54(5)
	1650.199	444.638	1
	2585.453	463.937	0.09(1)
	4437.558	507.562	0.033(7)
	5487.657	536.147	0.48(7)
	6005.271	551.455	0.016(5)
	6931.800	581.157	0.15(2)
	8420.321	636.209	0.06(1)
	10337.097	724.597	0.08(3)
	10883.260	754.462[b]	w
	10942.012	757.822[b]	
	11580.863	796.390	w
24321.262	0.000	411.047	1
	513.322	419.910	0.19(3)
	1470.097	437.492[a]	0.45(5)

Table 2. (*continued*).

Upper level energy (cm^{-1})	Lower level energy (cm^{-1})	Wavelength in air (nm)	Relative intensity
	1650.199	*440.968*[e]	*0.015(2)*
	3066.750	470.357	0.45(6)
	4437.558	502.785	0.21(2)
	6005.271	545.820	0.056(8)
	6931.800	574.902	0.11(1)
	8420.321	628.721	0.08(1)
	9908.650	693.646	0.09(2)
	10667.012	732.160[b]	0.024(7)
	10720.295	735.041[b]	
	12222.185	826.283	0.11(3)
24445.389	513.322	417.732	1
	1470.097	435.128	0.31(3)
	1650.199	438.566[a]	0.61(6)
	4437.558	499.665	0.031(5)
	5487.657	527.343	0.37(4)
	6005.271	542.146	0.019(4)
	6931.800	570.827	0.13(1)
	8420.321	623.850	0.038(8)
24468.033	0.000	408.581	1
	513.322	417.337[a]	0.45(5)
	1650.199	438.131	0.029(4)
	6005.271	541.480	0.18(2)
	7524.740	590.041	0.14(2)
	8796.378	637.919	0.041(9)
	9674.844	675.801	0.06(1)
24842.878	513.322	410.907	1
	1470.097	427.728[a]	0.056(7)
	1650.199	431.050	0.061(8)
	2585.453	449.163	0.031(4)
	3066.750	459.091	0.017(3)
	4512.481	491.738	0.046(6)
	5487.657	516.513	0.14(1)
	6931.800	558.159	0.048(6)
	7950.070	593.905	0.010(2)
	8420.321	608.751	0.011(2)
	9877.173	668.010	0.011(3)
	10942.012	719.182	0.017(4)
	11580.863	753.827	0.039(7)
	12021.350	780.157	0.020(5)
	12276.210	795.538	0.026(6)
24913.863	0.000	401.270	1
	513.322	409.712	0.031(4)
	1650.199	429.734[a]	0.15(2)
	6005.271	528.713	0.13(2)
	7524.740	574.913	0.08(1)
	8420.321	606.131	0.021(5)
	8796.378	620.273	0.028(9)
	9198.395	636.141	0.07(1)
	9674.844	656.030	0.04(1)
	9908.650	666.252	0.06(1)

Table 2. (*continued*).

Upper level energy (cm^{-1})	Lower level energy (cm^{-1})	Wavelength in air (nm)	Relative intensity
	10883.260	712.532[b]	0.05(1)
	10887.246	712.735[b]	
25080.880	513.322	406.927	1
	1470.097	423.417	0.037(5)
	1650.199	426.671[a]	0.39(4)
	2585.453	444.411	0.03(1)
	3066.750	454.127	0.58(6)
	4437.558	484.284[b]	0.026(5)
	4512.481	486.048[b]	
	5487.657	510.239	0.34(4)
	6931.800	550.840	0.10(1)
25138.556	0.000	397.683	1
	513.322	405.973	0.036(5)
	1650.199	425.623[a]	0.084(9)
	6005.271	522.504	0.12(1)
	7524.740	567.579	0.063(9)
25200.913	513.322	404.948	0.11(1)
	1470.097	421.275	0.22(2)
	1650.199	424.496[a]	0.17(2)
	2585.453	442.052	0.20(2)
	3066.750	451.664	0.21(2)
	4512.481	483.227	1
	5487.657	507.132	0.035(7)
	8009.810	581.536	0.07(1)
	9357.906	631.020	0.08(2)
	10786.783	693.935	0.11(3)
	12906.575	811.873	w
	13703.425	*869.507*[c]	*0.05(1)*
25295.288	0.000	395.219	1
	513.322	403.406	0.08(1)
	1650.199	422.802[a]	0.20(2)
	6005.271	518.259	0.18(2)
	7524.740	562.573	0.12(2)
	9198.395	621.066	0.03(1)
	9674.844	640.010	0.03(1)
	9877.173	648.736[b]	0.035(9)
	9908.650	649.736[b]	
	10887.246	693.866	0.08(4)
25352.384	513.322	402.478	1
	1470.097	418.603[a]	0.32(3)
	2585.453	439.111	0.33(3)
	3066.750	448.594	0.20(2)
	4512.481	479.715	0.78(8)
	5487.657	503.265	0.10(1)
	6931.800	542.721	0.028(8)
	7950.070	574.478	0.14(2)
	9357.906	625.044	0.12(2)
	11087.765	700.843	0.12(3)
	19703.435	*858.203*[c]	*0.015(4)*

Table 2. (*continued*).

Upper level energy (cm^{-1})	Lower level energy (cm^{-1})	Wavelength in air (nm)	Relative intensity
25389.217	0.000	393.757	0.13(1)
	513.322	401.882	0.61(6)
	1470.097	417.958[a]	1
	1650.199	421.129	0.59(6)
	3066.750	447.854	0.051(6)
	6931.800	541.637	0.18(2)
	7524.740	559.615	0.010(2)
	8420.321	589.151	0.14(2)
	9198.395	617.464	0.014(3)
	9877.173	644.483[b]	
	9908.650	645.793[b]	0.030(5)
	10054.195	651.923[b]	
	10667.120	679.049[b]	0.055(8)
	10720.295	681.526[b]	
25481.274	513.322	400.401	1
	1470.097	416.356	0.026(6)
	1650.199	419.502	0.61(6)
	2585.453	436.639[a]	0.23(3)
	3066.750	446.015	0.06(1)
	4437.558	475.069[b]	0.07(1)
	4512.481	476.767[b]	
	5487.657	500.021	0.049(8)
	10941.995	*687.603*[c]	*0.015(4)*
	11580.863	719.206	0.11(3)
	12021.350	742.742	0.09(4)
25524.485	1470.097	415.608	1
	2585.453	435.816	0.39(4)
	3066.750	445.156[a]	0.60(6)
	3801.930	*460.224*[d]	*0.010(5)*
	5487.657	498.942	0.038(8)
	5985.571	*511.657*[e]	*0.0036(5)*
	6637.411	529.316	0.38(4)
	6931.800	*537.697*[e]	*0.009(1)*
	7950.070	568.852	0.16(2)
	9357.906	*618.390*[e]	*0.025(3)*
25877.176	0.000	386.332	0.25(3)
	513.322	394.151	1
	1470.097	409.602	0.020(5)
	1650.199	412.647	0.035(6)
	3066.750	438.273[a]	0.08(1)
	4437.558	466.296	0.023(6)
	6931.800	527.687	0.12(1)
	8420.321	572.683	0.061(9)
	9357.906	605.187	0.026(9)
	9877.173	624.827	0.04(1)
	10666.777	*657.264*[c]	*0.007(2)*
26031.487	2585.453	426.392[a]	0.24(3)
	3801.930	449.726	0.32(3)
	4512.481	464.576	1

Table 2. (*continued*).

Upper level energy (cm^{-1})	Lower level energy (cm^{-1})	Wavelength in air (nm)	Relative intensity
	5085.619	477.288	0.43(4)
	5985.571	498.716	0.82(9)
	10194.786	631.272	0.07(2)
	12334.216	*729.872*[c]	*0.028(7)*
26274.095	513.322	388.077	1
	1470.097	403.047	0.38(5)
	1650.199	405.995	0.62(7)
	2585.453	422.025[a]	0.30(4)
	3066.750	430.777	0.21(3)
	7950.070	545.580	0.15(2)
	9357.906	590.986	0.10(1)
	10883.260	649.558	0.035(8)
	11580.863	680.398	0.12(2)
	12021.350	701.426[b]	0.020(7)
	12028.460	701.776[b]	
	12276.210	714.197	0.04(1)
	13597.857	*788.660*[c]	*0.006(2)*
26328.010	1470.097	402.173	1
	3066.750	429.778[a]	0.25(3)
	5487.657	479.704	0.017(3)
	6637.411	507.715	0.10(1)
	7950.070	543.980[b]	0.026(4)
	8009.810	545.754[b]	
	9042.743	578.368	0.044(6)
	10337.097	625.182	0.023(7)
	12906.575	744.871	0.015(2)
	13298.888	767.300	0.003(1)
	13597.857	785.320[b]	0.006(1)
	13615.183	786.483[b]	
26761.110	513.322	380.877	1
	1470.097	395.286	0.9(1)
	1650.199	398.121	0.50(6)
	2585.453	413.523	0.11(2)
	3066.750	421.923	0.05(1)
	4512.481	449.340[a]	0.26(3)
	7950.070	531.455	0.09(2)
	11580.863	658.570	0.15(4)
	13298.888	742.616	0.4(1)
26772.093	513.322	380.717	0.049(8)
	1470.097	395.114	1
	1650.199	397.947	0.46(5)
	2585.453	413.335	0.33(4)
	3066.750	421.727[a]	0.07(1)
	4512.481	*449.119*[e]	*0.009(1)*
	7950.070	531.145	0.21(3)
	8420.321	*544.756*[d]	*0.016(8)*
	9357.906	574.086	0.14(2)
	10337.097	*608.296*[d]	*0.03(2)*
	11580.863	658.093	w

Table 2. (*continued*).

Upper level energy (cm^{-1})	Lower level energy (cm^{-1})	Wavelength in air (nm)	Relative intensity
	11709.600	663.719	w
26912.765	2585.453	410.945	1
	3801.930	432.576[a]	0.32(3)
	4512.481	446.298	0.38(4)
	6637.411	493.073	0.024(6)
	7868.896	524.958[b]	0.32(3)
	7950.070	527.205[b]	
	9042.743	559.442	0.14(2)
	10337.097	603.127	0.05(1)
26991.889	513.322	377.557	0.17(3)
	1470.097	391.712	0.15(2)
	1650.199	394.495	0.054(7)
	2585.453	409.612	1
	3066.750	417.853[a]	0.28(3)
	4512.481	444.727	w
	8009.810	526.666	0.10(1)
	9357.906	566.930	0.07(1)
	10883.260	620.613[b]	0.06(2)
	10942.012	622.885[b]	
27445.854	2585.453	402.133	1
	3801.930	422.823[a]	0.048(6)
	4512.481	435.924	0.10(1)
	5085.619	447.098	0.10(1)
	7950.070	512.789	0.15(2)
	9042.743	543.236	0.063(8)
	10194.805	579.515	0.059(8)
	10337.097	584.335	0.08(3)
	11373.472	622.014	0.10(3)
	12459.978	667.112	0.13(4)
	14301.805	760.592	0.12(4)
27448.715	1470.097	384.823	1
	2585.453	402.086	0.98(3)
	3066.750	410.024	0.21(2)
	3801.930	422.772[a]	0.42(4)
	4512.481	435.869	0.15(2)
	6637.411	480.375	0.032(6)
	9042.743	543.152	0.23(2)
	10337.097	584.237	0.16(2)
	12906.575	687.467	0.12(2)
27611.719	2585.453	399.467	1
	3801.917	419.877	0.023(3)
	4512.481	432.793[a]	0.25(3)
	6637.411	476.641	0.012(2)
	7868.896	506.372	0.12(1)
	9042.743	538.383	0.022(3)
	10194.805	573.995	0.043(5)
	11373.472	615.660	0.013(2)
	12327.030	654.069[b]	0.006(1)
	12334.216	654.377[b]	

Table 2. (*continued*).

Upper level energy (cm^{-1})	Lower level energy (cm^{-1})	Wavelength in air (nm)	Relative intensity
	14301.805	751.113	0.029(4)
	14957.611	790.039	0.014(3)
	15357.954	*815.851*[e]	*0.006(1)*
27816.793	2585.453	396.221	1
	5085.619	439.801	0.06(7)
	5985.571	457.931[a]	0.8(8)
	7868.896	501.167	0.2(3)
	9042.743	532.503	0.06(7)
	10337.097	571.934	0.06(7)
27993.254	3801.930	413.255	0.16(2)
	5085.619	436.414[a]	0.33(3)
	5985.571	454.260	1
	9166.209	531.004	0.13(1)
	10194.786	561.692	0.052(8)
	11392.171	602.205	0.048(9)
	12459.978	643.603	0.06(1)
	16295.726	*854.648*[e]	*0.017(3)*
	16610.554	*878.286*[e]	*0.013(2)*
28196.156	2585.453	390.351	0.20(2)
	3066.750	397.828	0.20(2)
	3801.930	409.817	1
	4512.481	422.113[a]	0.42(4)
	9042.743	521.956	0.09(1)
	10337.097	559.785	0.08(1)
28285.619	1470.097	372.813	0.42(4)
	1650.199	375.334	0.041(7)
	2585.453	388.993	1
	3067.000	396.417	0.09(1)
	4512.534	420.525[a]	0.13(1)
	7950.070	491.613[b]	0.028(5)
	8009.810	493.062[b]	
	9877.173	543.078	0.046(7)
	10337.097	556.995	0.058(8)
	10941.995	576.421	0.08(1)
	12887.081	649.234	0.05(1)
28354.410	1470.097	371.859	0.12(1)
	2585.453	387.954	1
	3066.750	395.338	0.20(2)
	3801.917	407.176	0.13(1)
	5985.571	446.925[a]	0.26(3)
	9042.743	517.678	0.13(1)
	10337.097	554.868	0.09(1)
	11580.863	596.012	0.04(1)
	12887.081	646.346[b]	0.08(2)
	12906.575	647.161[b]	
28418.965	3801.930	406.108	1
	5085.619	428.451[a]	0.21(2)
	5985.571	445.639	0.17(2)
	7868.896	486.481	0.039(6)
	9166.209	519.261	0.30(3)

Table 2. (*continued*).

Upper level energy (cm^{-1})	Lower level energy (cm^{-1})	Wavelength in air (nm)	Relative intensity
	10194.805	548.570	0.15(2)
	11373.472	586.503	0.057(9)
	12459.978	*626.434*[d]	*0.004(2)*
28540.957	2585.453	385.166	1
	3801.930	404.106	0.9(1)
	4512.481	416.056	0.9(1)
	5085.619	426.223[a]	0.13(3)
	5985.571	443.229	0.15(4)
	10194.805	544.922	0.27(4)
	11373.472	582.336	0.18(3)
	13298.888	655.898	0.14(5)
	14301.805	702.096	0.25(8)
28748.524	3801.930	400.743	1
	5085.619	422.484[a]	0.34(4)
	5985.571	439.187	0.040(6)
	7868.896	478.803	0.053(7)
	9042.743	*507.324*[e]	*0.010(2)*
	9166.209	510.523	0.37(4)
	10194.805	538.826	0.09(1)
	11392.171	575.999	0.038(7)
	16610.554	823.635	w
	17001.500	851.048	w
28856.898	2585.453	380.534	0.62(7)
	3801.930	399.010	1
	4512.481	410.656	0.08(1)
	5085.619	420.558[a]	0.25(3)
	5985.571	437.106	0.030(8)
	7868.896	476.330[b]	
	7950.070	478.180[b]	0.021(9)
	8009.810	479.550[b]	
	10194.805	535.697	0.22(3)
	11373.472	571.812	0.11(2)
	13298.888	642.578	w
29027.543	3801.930	396.311	1
	5085.619	417.560[a]	0.30(3)
	5985.571	433.869	0.36(4)
	7868.896	472.489	0.021(5)
	9166.209	503.351	0.12(1)
	10194.786	530.843	0.040(7)
	11392.171	566.886	0.12(1)
	12459.978	603.423	0.09(1)
	14301.794	678.896	0.005(4)
	14481.957	687.305	0.02(1)
	15749.198	752.900	0.03(2)
	16610.554	805.127	0.06(4)
29434.270	1470.097	357.499	0.033(7)
	2585.453	372.350	0.38(5)
	3066.750	379.147	0.03(1)
	3801.930	390.022	1
	4512.481	*401.142*[e]	*0.012(1)*

Table 2. (*concluded*).

Upper level energy (cm^{-1})	Lower level energy (cm^{-1})	Wavelength in air (nm)	Relative intensity
	5985.571	426.343[a]	0.16(2)
	10941.995	540.617	0.050(7)
	11373.472	553.532	0.048(7)
	12021.350	574.127	0.025(6)
	12334.216	584.632	0.014(5)
	14259.383	658.802	0.020(9)
29955.418	3801.930	382.250	0.38(4)
	4512.481	392.926	1
	5085.619	401.981	0.72(8)
	5985.571	417.074[a]	0.24(3)
	7950.070	454.308	0.14(2)
	8009.810	455.545	0.03(1)
	10194.786	505.917	0.11(2)
	11373.472	538.008	0.08(1)
	12459.978	571.420	0.05(1)
	13298.888	600.199	0.08(2)
	14259.383	636.928	0.08(2)
	14387.400	642.166	0.10(2)
	14957.611	666.580	0.09(2)

[a]Transition used to excite the upper level.
[b]Blended line in this work.
[c]Transition observed by ref. 12, but not in this work.
[d]Transition observed by ref. 14, but not in this work.
[e]Transition observed by ref. 21, but not in this work.

Repeated calibrations spanning several months were rescaled with a least-squares procedure to minimize the residuals summed over wavelength, and showed very little change with time in the relative spectral efficiency of our system. An empirical estimate of the uncertainty in our measurement of the relative detection efficiency was obtained by examining the relative intensity of all spectral lines that were common to two or more scans, each taken with a different grating. This test exposed any scatter greater than that expected from the statistical uncertainty obtained from the repeated calibrations. Such excess scatter can only be due to systematic effects in our calibration, which would not be evident in the relative calibrations. We found that the average magnitude of this excess was ∼3%. The use of both optical fiber bundles during the calibration procedure introduced an additional 0.2% uncertainty due to a slightly increased attenuation during the calibration not present during branching-fraction measurement. This value is combined with the 3.0% calibration procedure uncertainty to derive a total uncertainty of 3.2%, which appears in Table 1 as "(systematic) efficiency calibration procedure".

Estimates of the uncertainties in our determination of the relative intensities of radiative transitions in Nd II are summarized in Table 1. The total uncertainty was obtained by combining in quadrature the statistical uncertainty from the fitting and calibration procedures with the systematic uncertainty from the efficiency calibration (including lamp calibration). Repeated measurements of the relative intensities of branches from a single upper level taken over many months yielded deviations of less than 1% for the large branches (branching fractions larger than 0.1) and less than 3% for the smaller branches. The excellent repeatability and self-consistency of these measurements confirms that the systematic uncertainty in the relative efficiency calibration dominates the error budget.

Table 3. Transition probabilities and oscillator strengths derived from branching-fraction and lifetime data. Data from this work are compared with those of refs. 14, 19, and 21. Branches that were observed but were too small to fit are indicated by "w" if they are listed in other references.

					$g_u A_{ul}$ (10^6 s^{-1})				
Upper level energy (cm^{-1})[a]	J	τ_u (ns)	Transition wavelength (nm)	Branching fraction	This work	DLSC[e]	XSCLQB[f]	MW[g]	$\log(g_l f_{lk})$ This work
22696.885	5.5	80.6(4.7)[b]	450.659	0.180(13)	26.8(2.5)	29.8(1.7)	25.87		–1.077
			470.971	0.189(13)	27.8(2.5)	32.4(1.8)	36.83		–1.019
			475.002	0.0131(12)	1.95(21)	2.41(22)			
			497.092	0.0600(48)	8.93(88)	10.92(72)	14.88		–1.472
			509.280	0.364(20)	54.2(4.4)	63.5(3.2)	55.57		–0.667
			547.514	0.0065(9)	0.97(15)				–2.371
			580.923	0.0351(29)	5.22(53)	3.84(72)			–1.576
			634.139	0.0234(24)	3.48(41)	3.18(31)			–1.683
			700.257	0.0159(33)	2.36(51)				–1.783
			749.478	0.0108(32)	1.61(48)				–1.889
			779.835	0.046(11)	6.8(1.7)				–1.230
			808.854	0.0152(49)	2.27(75)				–1.676
			850.478	0.044(18)	6.5(2.7)	1.91(25)			–1.174
22850.552	3.5	85.6(1.4)[b]	437.503	0.281(17)	26.3(1.6)	27.8(1.7)			–1.122
			447.558	0.0653(50)	6.11(48)				–1.736
			471.559	0.319(18)	29.8(1.8)	37.9(2.0)			–1.002
			593.474	0.0498(41)	4.65(39)				–1.610
			652.314	0.0721(60)	6.74(57)				–1.366
			692.799	0.0359(41)	3.36(39)				–1.617
			711.336	0.0041(7)	0.39(7)				–2.533
			732.284	0.0123(18)	1.15(17)				–2.035
			758.764	0.0404(56)	3.77(53)				–1.487
			772.472	0.0194(36)	1.82(34)				–1.789
			820.539	0.0550(76)	5.14(72)				–1.285
			835.660	0.0455(67)	4.25(63)				–1.351

Table 3. (*continued*).

Upper level Energy (cm^{-1})[a]	J	τ_k (ns)	Transition wavelength (nm)	Branching fraction	$g_u A_{ul}$ (10^6 s^{-1}) This work	DLSC[e]	XSCLQB[f]	MW[g]	$\log(g_i f_{ik})$ This work
23159.979	5.5	79.6(2.5)[b]	441.443	0.073(11)	11.0(1.7)	8.88(48)			–1.493
			460.916	0.0166(50)	2.51(75)	1.58(18)			–2.098
			464.775	0.0537(81)	8.1(1.2)	6.24(36)			–1.581
			485.903	0.667(28)	100.5(4.3)	103.2(4.8)			–0.449
			536.117	0.060(15)	9.0(2.3)	7.68(72)			–1.410
			752.646	0.0198(59)	2.99(89)				–1.595
			779.642	0.0230(76)	3.5(1.1)				–1.501
			814.326[d]	0.088(19)	13.2(2.8)				–0.882
			818.241[d]						
23229.991	4.5	13.3(4)[b]	430.357	0.603(20)	454(20)	437 (23)	448.3	470.0	0.101
			440.082	0.0945(76)	71.1(6.1)	86.0(5.0)	34.80	68.0	–0.685
			463.267	0.0144(15)	10.8(1.2)	9.40(70)	22.68	10.0	–1.458
			495.814	0.0195(17)	14.7(1.4)	15.5(1.0)	16.84	12.0	–1.266
			531.982	0.192(14)	144 (11)	172 (13)	165.6	156.0	–0.213
			580.400	0.0568(46)	42.7(3.7)	59.0(5.0)	48.31	46.0	–0.666
			613.396	0.0052(6)	3.91(48)			2.0	–1.656
			636.554	0.0143(14)	10.8(1.1)	10.3(1.2)	5.983	7.0	–1.184
23397.385	3.5	66.6(1.1)[b]	427.278	0.185(13)	22.2(1.6)	26.5(1.4)			–1.217
			436.863	0.380(20)	45.6(2.5)	54.4(2.4)			–0.884
			459.701	0.157(11)	18.8(1.4)	22.6(1.2)			–1.224
			574.814	0.0670(53)	8.04(65)				–1.399
			629.841	0.079(12)	9.5(1.4)	6.32(56)			–1.247
			684.696	0.0466(79)	5.60(96)				–1.405
			704.083	0.0136(14)	1.63(17)				–1.916
			728.528	0.0503(96)	6.0(1.2)				–1.318
			741.156	0.0113(13)	1.36(16)				–1.952
			798.878[d]	0.0114(18)	1.37(22)				–1.883
			799.133[d]						

Table 3. (*continued*).

Upper level energy (cm^{-1})[a]	J	τ_k (ns)	Transition wavelength (nm)	Branching fraction	$g_u A_{ul}$ (10^6 s^{-1}) This work	DLSC[e]	XSCLQB[f]	MW[g]	$\log(g_i f_{ik})$ This work
23409.537	4.5	70.5(3.8)[b]	427.057	0.1289(90)	18.3(1.6)	19.8(1.2)			–1.301
			436.632	0.1106(79)	15.7(1.4)	15.7(1.0)			–1.348
			455.673	0.1074(77)	15.2(1.4)	14.50(80)			–1.324
			459.445	0.1000(73)	14.2(1.3)	13.70(80)			–1.348
			491.438	0.359(18)	50.9(3.7)	54.7(2.8)			–0.734
			526.947	0.0725(76)	10.3(1.2)				–1.368
			574.413	0.0330(37)	4.68(58)				–1.635
			606.713	0.0151(19)	2.15(29)				–1.926
			629.360	0.0079(9)	1.12(14)				–2.179
			666.963	0.0180(22)	2.56(35)				–1.768
			703.481[d]	0.0071(9)	1.01(14)				–2.125
			711.467[d]						
			738.767[d]	0.0092(12)	1.31(19)				–1.970
			740.489[d]						
			784.545[d]	0.0225(28)	3.19(43)				–1.530
			787.854[d]						
			798.103	0.0086(16)	1.22(24)				–1.932
23537.387	4.5	26.6(5)[b]	424.737	0.507(22)	190.6(9.0)	227(12)			–0.288
			434.206	0.0550(45)	20.7(1.8)	23.2(1.6)			–1.233
			453.033	0.0189(18)	7.10(69)				–1.660
			456.761	0.0401(35)	15.1(1.3)	15.8(1.0)			–1.326
			488.369	0.0158(16)	5.92(61)				–1.674
			523.419	0.172(13)	64.7(5.1)	74.0(5.0)			–0.575
			570.224	0.0731(64)	27.5(2.4)	27.3(2.1)			–0.872
			624.334	0.0255(36)	9.6(1.3)	3.50(40)			–1.251
			697.207	0.0075(18)	2.82(69)				–1.687
			731.852[d]	0.0064(19)	2.39(70)				–1.716
			733.542[d]						
			845.236	0.079(18)	29.6(6.9)				–0.499

Table 3. (*continued*).

Upper level Energy (cm^{-1})[a]	J	τ_k (ns)	Transition wavelength (nm)	Branching fraction	$g_u A_{ul}$ (10^6 s^{-1}) This work	DLSC[e]	XSCLQB[f]	MW[g]	$\log(g_i f_{ik})$ This work
23857.278	5.5	66.1(2.4)[b]	428.257	0.1271(89)	23.1(1.8)	22.3(1.7)			–1.197
			446.560	0.150(10)	27.3(2.1)	26.6(1.9)			–1.088
			450.181	0.331(18)	60.2(3.9)	68.4(4.8)			–0.738
			516.792	0.1084(86)	19.7(1.7)	16.4(1.6)			–1.103
			544.226	0.152(11)	27.7(2.3)				–0.911
			590.662	0.0870(75)	15.8(1.5)				–1.083
			647.618	0.0263(50)	4.77(93)				–1.522
			715.106	0.0172(40)	3.13(74)				–1.620
24053.354	4.5	74.3(4.0)[b]	415.626	0.220(14)	29.6(2.5)	33.5(1.9)			–1.115
			424.689	0.0469(40)	6.31(64)	6.10(40)			–1.768
			442.682	0.0479(40)	6.45(64)	6.00(40)			–1.722
			446.241	0.320(18)	43.1(3.4)	40.8(2.2)			–0.891
			476.362	0.1151(93)	15.5(1.5)	15.90(90)			–1.278
			509.652	0.102(10)	13.7(1.6)				–1.272
			553.922	0.0332(49)	4.47(70)				–1.686
			583.898	0.0091(36)	1.23(48)				–2.201
			604.845	0.0067(36)	0.90(48)				–2.304
			639.495	0.0153(48)	2.07(65)				–1.897
			705.214	0.0188(65)	2.53(89)				–1.724
			746.813[d]	0.0102(47)	1.37(64)				–1.940
			749.810[d]						
			762.489	0.0098(40)	1.32(54)				–1.940
			809.906	0.0162(79)	2.2(1.1)				–1.668
			830.889[d]	0.0123(65)	1.65(87)				–1.767
			835.459[d]						
			844.994[d]	0.0162(89)	2.2(1.2)				–1.632
			845.745[d]						
			848.871[d]						

Table 3. (*continued*).

Upper level energy (cm^{-1})[a]	J	τ_k (ns)	Transition wavelength (nm)	Branching fraction	$g_u A_{ul}$ (10^6 s^{-1}) This work	DLSC[e]	XSCLQB[f]	MW[g]	$\log(g_i f_{ik})$ This work
24134.095	5.5	24.6(5)[b]	423.237	0.224(15)	109.1(7.5)	126 (11)			–0.533
			441.105	0.156(11)	75.9(5.6)	86.4(7.2)			–0.655
			444.638	0.292(18)	142.5(9.1)	150 (12)			–0.374
			463.937	0.0263(29)	12.8(1.4)	11.52(96)			–1.383
			507.562	0.0111(22)	5.4(1.1)				–1.676
			536.147	0.168(18)	81.7(8.9)				–0.453
			551.455	0.0057(19)	2.76(93)				–1.899
			581.157	0.0571(78)	27.9(3.9)	27.2(3.1)			–0.850
			636.209	0.0251(53)	12.3(2.6)				–1.128
			724.597	0.036(13)	17.4(6.2)				–0.862
24321.262	4.5	51.7(7.1)[b]	411.047	0.311(19)	60.3(9.1)	77.0(4.0)			–0.816
			419.910	0.0619(67)	12.0(2.1)	11.40(80)			–1.500
			437.492	0.149(13)	28.8(4.7)	29.3(1.7)			–1.082
			470.357	0.160(15)	30.9(5.2)	30.5(1.9)			–0.989
			502.785	0.0816(69)	15.8(2.5)	17.2(1.3)			–1.223
			545.820	0.0232(30)	4.50(85)				–1.697
			574.902	0.0476(49)	9.2(1.6)	7.90(80)			–1.340
			628.721	0.0361(53)	7.0(1.4)	4.50(50)			–1.383
			693.646	0.0494(93)	9.6(2.2)	4.30(60)			–1.161
			732.160[d]	0.0133(40)	2.57(85)				–1.685
			735.041[d]						
			826.283	0.067(19)	12.9(4.0)				–0.879
24445.389	5.5	15.62(21)[c]	417.732	0.365(19)	280 (15)	302 (17)			–0.134
			435.128	0.1187(85)	91.2(6.7)	86.4(6.0)			–0.587
			438.566	0.235(15)	180(12)	175 (11)			–0.283
			499.665	0.0137(18)	10.5(1.4)				–1.360
			527.343	0.172(12)	132.1(9.6)	157.2(12.0)			–0.259
			542.146	0.0091(19)	7.0(1.5)				–1.511
			570.827	0.0658(58)	50.5(4.5)				–0.607
			623.850	0.0210(38)	16.1(2.9)				–1.027

Table 3. (*continued*).

Upper level Energy (cm^{-1})[a]	J	τ_k (ns)	Transition wavelength (nm)	Branching fraction	$g_u A_{ul}$ (10^6 s^{-1}) This work	DLSC[e]	XSCLQB[f]	MW[g]	$\log(g_i f_{ik})$ This work
24468.033	3.5	166(18)[c]	408.581	0.478(21)	23.1(1.0)	27.4(1.4)			–1.239
			417.337	0.219(15)	10.6(7)	12.24(72)			–1.559
			438.131	0.0150(19)	0.72(9)				–2.681
			541.480	0.1139(90)	5.49(44)	5.44(56)			–1.617
			590.041	0.0991(85)	4.78(41)				–1.603
			637.919	0.0303(63)	1.46(31)				–2.049
			675.801	0.0439(95)	2.12(46)				–1.839
24842.878	5.5	31.6(2.1)[b]	410.907	0.585(20)	222 (17)	271 (14)			–0.249
			427.728	0.0341(39)	12.9(1.7)	11.88(84)			–1.450
			431.050	0.0377(42)	14.3(1.8)	13.4(1.1)			–1.399
			449.163	0.0197(21)	7.50(93)	6.96(60)			–1.644
			459.091	0.0112(18)	4.26(74)				–1.870
			491.738	0.0320(34)	12.2(1.5)	9.96(72)			–1.355
			516.513	0.1016(87)	38.6(4.2)	45.6(4.8)			–0.811
			558.159	0.0380(45)	14.4(2.0)	13.9(1.4)			–1.171
			593.905	0.0084(18)	3.21(73)				–1.774
			608.751	0.0092(20)	3.51(79)				–1.710
			668.010	0.0103(24)	3.91(94)				–1.583
			719.182	0.0179(36)	6.8(1.5)				–1.277
			753.827	0.0421(72)	16.0(2.9)				–0.865
			780.157	0.0224(52)	8.5(2.1)				–1.110
			795.538	0.0298(68)	11.3(2.7)				–0.969
24913.863	3.5	61.0(3.7)[b]	401.270	0.527(26)	69.1(5.4)	104.8(5.6)			–0.778
			409.712	0.0167(18)	2.19(27)				–2.258
			429.734	0.0819(81)	10.7(1.2)	10.88(64)			–1.526
			528.713	0.0927(96)	12.2(1.5)				–1.293
			574.913	0.0609(85)	8.0(1.2)				–1.402
			606.131	0.0169(39)	2.22(53)				–1.913

Table 3. (*continued*).

Upper level energy (cm^{-1})[a]	J	τ_k (ns)	Transition wavelength (nm)	Branching fraction	$g_u A_{ul}$ (10^6 s^{-1}) This work	DLSC[e]	XSCLQB[f]	MW[g]	$\log(g_i f_{ik})$ This work
			620.273	0.0227(72)	2.98(97)				–1.765
			636.141	0.057(10)	7.5(1.4)				–1.344
			656.030	0.0336(96)	4.4(1.3)				–1.546
			666.252	0.048(11)	6.3(1.5)				–1.376
			712.532[d]	0.043(13)	5.6(1.7)				–1.370
			712.735[d]						
25080.880	5.5	39.5(2.4)[b]	406.927	0.368(20)	111.9(9.1)	107(11)			–0.556
			423.417	0.0142(18)	4.31(60)				–1.936
			426.671	0.151(11)	45.8(4.3)	39.6(3.6)			–0.903
			444.411	0.0137(38)	4.2(1.2)	3.17(36)			–1.908
			454.127	0.238(17)	72.4(6.7)	58.8(6.0)			–0.650
			484.284[d]	0.0116(18)	3.52(60)				–1.908
			486.048[d]						
			510.239	0.155(12)	47.1(4.5)				–0.736
			550.840	0.0480(46)	14.6(1.7)				–1.178
25138.556	3.5	34.2(1.4)[c]	397.683	0.727(18)	170.2(8.1)	168.0(8.8)			–0.394
			405.973	0.0265(32)	6.19(80)	5.28(40)			–1.815
			425.623	0.0655(62)	15.3(1.6)	14.32(88)			–1.381
			522.504	0.115(11)	26.9(2.8)				–0.958
			567.579	0.0658(81)	15.4(2.0)				–1.129
25200.913	5.5	98.3(9.4)[c]	404.948	0.0437(41)	5.33(71)				–1.882
			421.275	0.0879(69)	10.7(1.3)				–1.544
			424.496	0.0679(55)	8.3(1.0)				–1.650
			442.052	0.0843(71)	10.3(1.3)				–1.521
			451.664	0.0878(74)	10.7(1.4)				–1.484
			483.227	0.454(22)	55.4(5.9)				–0.712
			507.132	0.0166(32)	2.03(44)				–2.107
			581.536	0.0373(58)	4.55(84)				–1.637

Table 3. (*continued*).

Upper level energy (cm^{-1})[a]	J	τ_k (ns)	Transition wavelength (nm)	Branching fraction	$g_u A_{ul}$ (10^6 s^{-1}) This work	DLSC[e]	XSCLQB[f]	MW[g]	$\log(g_i f_{ik})$ This work
			631.020	0.0500(90)	6.1(1.2)				–1.438
			693.935	0.070(17)	8.6(2.2)				–1.208
25295.288	3.5	30.64(63)[c]	395.219	0.498(26)	130.1(7.3)	172.0(8.8)			–0.516
			403.406	0.0432(43)	11.3(1.2)	7.60(48)			–1.560
			422.802	0.1041(89)	27.2(2.4)	25.5(1.8)			–1.137
			518.259	0.118(11)	30.8(3.0)	30.4(2.4)			–0.907
			562.573	0.0875(98)	22.9(2.6)	15.9(1.5)			–0.965
			621.066	0.0273(73)	7.1(1.9)	5.0(1.0)			–1.384
			640.010	0.022(10)	5.7(2.6)				–1.452
			648.736[d]	0.0284(71)	7.4(1.9)				–1.330
			649.736[d]						
			693.866	0.071(29)	18.6(7.5)	6.7(1.1)			–0.872
25352.384	5.5	59.9(2.3)[c]	402.478	0.278(17)	55.8(4.0)	57.8(3.1)			–0.868
			418.603	0.0938(71)	18.8(1.6)	18.6(1.1)			–1.306
			439.111	0.1001(75)	20.0(1.7)	19.6(1.2)			–1.237
			448.594	0.0621(50)	12.4(1.1)	12.00(96)			–1.425
			479.715	0.259(16)	51.9(3.8)	59.0(3.6)			–0.747
			503.265	0.0338(35)	6.77(74)				–1.590
			542.721	0.0105(31)	2.09(62)				–2.034
			574.478	0.0556(57)	11.1(1.2)				–1.258
			625.044	0.0507(71)	10.2(1.5)	7.44(96)			–1.225
			700.843	0.056(14)	11.2(2.8)				–1.083
25389.217	4.5	35.1(9)[b]	393.757	0.0403(32)	11.5(10)	12.40(70)			–1.573
			401.882	0.199(13)	56.7(4.0)	59.0(3.0)			–0.862
			417.958	0.338(18)	96.4(5.6)	87.0(4.0)			–0.598
			421.129	0.202(13)	57.5(4.0)	52.3(2.7)			–0.816
			447.854	0.0185(17)	5.27(51)	4.70(30)			–1.800
			541.637	0.0788(66)	22.4(2.0)				–1.005

Table 3. (*continued*).

Upper level energy (cm^{-1})[a]	J	τ_k (ns)	Transition wavelength (nm)	Branching fraction	$g_u A_{ul}$ (10^6 s^{-1}) This work	DLSC[e]	XSCLQB[f]	MW[g]	$\log(g_i f_{ik})$ This work
			559.615	0.0044(11)	1.25(31)				–2.232
			589.151	0.0663(63)	18.9(1.8)				–1.008
			617.464	0.0072(12)	2.05(36)				–1.930
			644.483[d]	0.0157(22)	4.48(64)				–1.555
			645.793[d]						
			651.923[d]						
			679.049[d]	0.0301(37)	8.6(1.1)				–1.227
			681.526[d]						
25481.274	5.5	50.6(2.0)[c]	400.401	0.402(25)	95.2(7.1)	111.6(9.6)			–0.635
			416.356	0.0106(6)	2.52(17)	1.07(19)			
			419.502	0.257(19)	61.0(5.2)	63.6(4.8)			–0.788
			436.639	0.1015(93)	24.1(2.4)				–1.159
			446.015	0.0276(40)	6.55(99)	6.96(60)			–1.708
			475.069[d]	0.0328(50)	7.8(1.2)				–1.578
			476.767[d]			6.96(72)			
			500.021	0.0247(35)	5.87(87)				–1.653
			719.206	0.076(22)	18.0(5.2)	15.2(2.3)			–0.850
			742.742	0.068(30)	16.1(7.2)				–0.870
25524.485	6.5	8.79(23)[b]	415.608	0.357(19)	569(34)	563(31)		481.6	0.168
			435.816	0.146(11)	232 (18)	241(15)		215.6	–0.179
			445.156	0.231(15)	368(26)	392 (24)		355.6	0.039
			460.222					5.6	
			498.942	0.0161(33)	25.6(5.3)	17.4(1.4)			–1.019
			529.316	0.174(12)	277(22)	297(22)		168.0	0.066
			568.852	0.0763(74)	121 (12)	102.2(9.8)		82.6	–0.230
			618.390			20.7(2.4)		5.6	
25877.176	4.5	14.4(1.4)[b]	386.332	0.140(11)	97.4(12.2)	117.0(7.0)		154.0	–0.661
			394.151	0.568(21)	394 (41)	413 (21)		608.0	–0.037

Table 3. (*continued*).

Upper level energy (cm^{-1})[a]	J	τ_k (ns)	Transition wavelength (nm)	Branching fraction	$g_u A_{ul}$ (10^6 s^{-1}) This work	DLSC[e]	XSCLQB[f]	MW[g]	$\log(g_i f_{ik})$ This work
			409.602	0.0118(28)	8.2(2.1)	3.20(40)		3.0	–1.687
			412.647	0.0208(32)	14.5(2.6)	11.20(90)		9.0	–1.432
			438.273	0.0500(52)	34.7(4.9)	31.6(2.9)		40.0	–1.000
			466.296	0.0155(39)	10.8(2.9)	6.50(70)			–1.454
			527.687	0.0876(85)	60.8(8.3)			119.0	–0.595
			572.683	0.0499(70)	34.7(5.9)	31.0(3.0)		56.0	–0.768
			605.187	0.0226(72)	15.7(5.2)			11.0	–1.064
			624.827	0.0338(91)	23.4(6.7)	15.3(2.3)			–0.862
26031.487	7.5	90.9(7.6)[b]	426.392	0.0762(61)	13.4(1.6)	9.44(64)			–1.437
			449.726	0.1055(81)	18.6(2.1)	13.6(1.1)			–1.249
			464.576	0.340(19)	59.8(6.0)	53.6(2.9)			–0.713
			477.288	0.149(11)	26.2(2.9)	25.9(2.1)			–1.048
			498.716	0.299(18)	52.7(5.4)	43.2(2.6)			–0.707
			631.272	0.0301(78)	5.3(1.4)				–1.499
26274.095	5.5	19.7(2.1)[b]	388.077	0.299(19)	182 (22)	215(11)			–0.385
			403.047	0.118(11)	71.8(10.2)	82.8(4.8)			–0.757
			405.995	0.195(15)	119(16)	123.6(7.2)			–0.533
			422.025	0.0991(98)	60.4(8.8)	60.0(3.6)			–0.792
			430.777	0.0710(80)	43.3(6.7)	43.6(3.2)			–0.919
			545.580	0.0632(63)	38.5(5.6)	40.8(3.6)			–0.764
			590.986	0.0436(49)	26.6(4.1)				–0.857
			649.558	0.0174(39)	10.6(2.6)				–1.172
			680.398	0.0615(87)	37.5(6.6)				–0.585
			701.426[d]	0.0106(37)	6.4(2.4)				–1.323
			701.776[d]						
			714.197	0.0217(52)	13.2(3.5)				–0.996
26328.010	6.5	42.7(3.1)[b]	402.173	0.629(20)	206 (16)	202(11)			–0.301
			429.778	0.169(13)	55.5(5.9)	54.0(3.4)			–0.813

Table 3. (*continued*).

Upper level energy (cm^{-1})[a]	J	τ_k (ns)	Transition wavelength (nm)	Branching fraction	$g_u A_{ul}$ (10^6 s^{-1}) This work	DLSC[e]	XSCLQB[f]	MW[g]	$\log(g_i f_{ik})$ This work
			479.704	0.0127(22)	4.18(78)				–1.841
			507.715	0.0767(68)	25.2(2.9)				–1.012
			543.980[d]	0.0218(35)	7.1(1.3)				–1.499
			545.754[d]						
			578.368	0.0395(52)	12.9(2.0)				–1.188
			625.182	0.0222(62)	7.3(2.1)				–1.371
			744.871	0.0169(20)	5.56(77)				–1.335
			767.300	0.0040(12)	1.30(39)				–1.940
			785.320[d]	0.0081(16)	2.65(56)				–1.611
			786.483[d]						
26761.110	5.5	35.4(1.4)[b]	380.877	0.246(21)	83.3(7.9)	103.2(6.0)			–0.742
			395.286	0.233(20)	78.8(7.5)	91.2(4.8)			–0.733
			398.121	0.127(13)	43.2(4.6)	52.3(2.9)			–0.988
			413.523	0.0292(44)	9.9(1.5)				–1.596
			421.923	0.0134(31)	4.5(1.1)	1.92(20)			–1.916
			449.340	0.0767(90)	26.0(3.2)	30.7(2.0)			–1.104
			531.455	0.0310(60)	10.5(2.1)	11.0(1.3)			–1.351
			658.570	0.064(16)	21.8(5.5)				–0.848
			742.616	0.179(48)	60.8(16.5)				–0.298
26772.093	5.5	11.1(9)[b]	380.717	0.0195(30)	21.1(3.7)	14.3(1.1)		58.8	–1.339
			395.114	0.412(20)	445(42)	472(24)		721.2	0.018
			397.947	0.189(13)	205(22)	198 (11)		326.4	–0.313
			413.335	0.143(11)	155(17)	125(7)		176.4	–0.401
			421.727	0.0316(42)	34.2(5.3)	20.3(1.3)		28.8	–1.040
			531.145	0.119(11)	128 (15)	90.0(7.2)		136.8	–0.265
			544.756					15.6	
			574.086	0.0857(96)	93(13)	60.0(6.0)		86.4	–0.339
			608.290					34.8	

Table 3. (*continued*).

Upper level energy (cm^{-1})[a]	J	τ_k (ns)	Transition wavelength (nm)	Branching fraction	$g_u A_{ul}$ (10^6 s^{-1}) This work	DLSC[e]	XSCLQB[f]	MW[g]	$\log(g_i f_{ik})$ This work
			658.093	w		22.0(2.6)			
			663.719	w		21.6(2.8)			
26912.765	5.5	7.31(15)[c]	410.945	0.408(20)	894 (47)	883 (48)		448.8	0.230
			432.576	0.137(10)	300 (23)	339(26)		186.0	–0.199
			446.298	0.169(12)	369 (27)	366(24)		214.8	–0.082
			493.073	0.0115(28)	25.3(6.1)				–1.161
			524.958[d]	0.166(12)	363 (27)	387 (30)		214.8	0.051
			527.205[d]						
			559.442	0.0766(70)	168(16)	149(13)		84.0	–0.229
			603.127	0.0317(64)	70(14)	33.3(3.4)		20.4	–0.546
26991.889	5.5	90.8(8.2)[c]	377.557	0.082(10)	10.8(1.7)	13.1(1.1)			–1.637
			391.712	0.0736(63)	9.7(1.2)	10.56(72)			–1.650
			394.495	0.0266(30)	3.52(51)	2.16(28)			–2.086
			409.612	0.514(23)	68.0(6.9)	72.0(3.6)			–0.767
			417.853	0.145(14)	19.2(2.5)	18.0(1.2)			–1.299
			526.666	0.0646(78)	8.5(1.3)				–1.450
			566.930	0.0508(85)	6.7(1.3)				–1.490
			620.613[d]	0.043(12)	5.7(1.7)				–1.480
			622.885[d]						
27445.854	7.5	36.1(1.6)[b]	402.133	0.429(28)	190 (15)	331(18)			–0.336
			422.823	0.0216(25)	9.6(1.2)	13.44(96)			–1.591
			435.924	0.0469(46)	20.8(2.2)	21.9(1.6)			–1.227
			447.098	0.0465(46)	20.6(2.3)	18.7(1.3)			–1.209
			512.789	0.0822(80)	36.4(3.9)				–0.842
			543.236	0.0363(44)	16.1(2.1)	16.6(2.2)			–1.148
			579.515	0.0367(48)	16.2(2.2)	14.6(1.8)			–1.087
			584.335	0.051(18)	22.5(7.9)				–0.939
			622.014	0.063(17)	28.0(7.8)				–0.789

Table 3. (*continued*).

Upper level energy (cm^{-1})[a]	J	τ_k (ns)	Transition wavelength (nm)	Branching fraction	$g_u A_{ul}$ (10^6 s^{-1}) This work	DLSC[e]	XSCLQB[f]	MW[g]	$\log(g_i f_{ik})$ This work
			667.112	0.089(24)	39.5(10.7)				–0.578
			760.592	0.098(29)	43.4(13.0)				–0.424
27448.715	6.5	16.6(9)[b]	384.823	0.270(16)	228(18)	251(14)			–0.296
			402.086	0.277(16)	233 (19)	265(14)			–0.247
			410.024	0.0602(47)	50.7(4.8)	53.9(2.9)			–0.893
			422.772	0.1257(90)	106.0(9.5)	117.6(7.0)			–0.546
			435.869	0.0471(38)	39.7(3.9)	40.2(2.8)			–0.946
			480.375	0.0106(18)	9.0(1.6)	8.26(84)			–1.508
			543.152	0.0868(68)	73.2(6.9)	75.6(7.0)			–0.490
			584.237	0.0640(57)	54.0(5.6)				–0.558
			687.467	0.0587(96)	49.5(8.5)				–0.455
27611.719	7.5	20.5(4)[b]	399.467	0.599(20)	467 (18)	458(24)			0.049
			419.877	0.0145(16)	11.3(1.3)	7.84(64)			–1.523
			432.793	0.165(12)	128 (10)	142.4(8.0)			–0.443
			476.641	0.0087(15)	6.8(1.2)				–1.637
			506.372	0.0911(81)	71.1(6.5)	61.9(4.6)			–0.563
			538.383	0.0177(22)	13.8(1.7)	12.6(1.4)			–1.222
			573.995	0.0368(39)	28.7(3.1)	23.5(2.7)			–0.847
			615.660	0.0121(19)	9.4(1.5)				–1.271
			654.069[d]	0.0058(11)	4.54(88)				–1.536
			654.377[d]						
			751.113	0.0330(38)	25.7(3.0)	23.8(3.0)			–0.662
			790.039	0.0170(32)	13.3(2.5)				–0.906
27816.793	7.5	55.8(1.7)[b]	396.221	0.419(22)	120.2(7.3)	113.6(6.4)			–0.548
			439.801	0.0295(36)	8.5(1.1)				–1.609
			457.931	0.364(21)	104.4(6.8)	104.0(6.4)			–0.483
			501.167	0.1189(98)	34.1(3.0)	27.4(2.2)			–0.891
			532.503	0.0330(53)	9.5(1.5)	6.24(96)			–1.395
			571.934	0.0350(66)	10.0(1.9)				–1.307

Table 3. (*continued*).

Upper level energy (cm^{-1})[a]	J	τ_k (ns)	Transition wavelength (nm)	Branching fraction	$g_u A_{ul}$ (10^6 s^{-1}) This work	DLSC[e]	XSCLQB[f]	MW[g]	$\log(g_i f_{ik})$ This work
27993.254	8.5	60.6(7.9)[b]	413.255	0.0798(67)	23.7(3.7)	31.7(2.7)			–1.217
			436.414	0.171(13)	50.7(7.6)	56.3(3.4)			–0.839
			454.260	0.546(21)	162 (22)	171.0(9.0)			–0.299
			531.004	0.0849(75)	25.2(4.0)	24.7(2.2)			–0.972
			561.692	0.0349(50)	10.4(2.0)				–1.310
			602.205	0.0351(63)	10.4(2.3)				–1.246
			643.603	0.0484(89)	14.4(3.2)				–1.049
28196.156	6.5	77.6(7.5)[b]	390.351	0.0933(81)	16.8(2.2)	20.3(1.4)			–1.415
			397.828	0.0958(81)	17.3(2.2)	18.3(1.3)			–1.387
			409.817	0.489(21)	88.2(9.3)	92.4(4.2)			–0.653
			422.113	0.210(15)	37.8(4.5)	37.0(2.1)			–0.996
			521.956	0.0573(66)	10.3(1.6)				–1.374
			559.785	0.0554(80)	10.0(1.7)				–1.328
28285.619	5.5	17.85(83)[c] *	372.813	0.194(14)	130 (11)	151.2(8.4)	50.64		–0.566
			375.334	0.0191(32)	12.9(2.2)	12.12(84)			–1.565
			388.993	0.486(21)	326 (20)	347(18)	378.9		–0.130
			396.417	0.0451(40)	30.3(3.1)	31.2(1.8)	64.48		–1.146
			420.525	0.0670(57)	45.1(4.4)	51.0(3.4)	49.00		–0.923
			491.613[d]	0.0173(27)	11.6(1.9)	8.64(84)			–1.376
			493.062[d]						
			543.078	0.0315(42)	21.1(3.0)				–1.029
			556.995	0.0400(50)	26.9(3.6)		15.89		–0.902
			576.421	0.0611(67)	41.1(4.9)				–0.689
			649.234	0.0393(78)	26.4(5.4)	20.8(2.8)	19.25		–0.777
28354.410	6.5	28.4(3.0)[b]	371.859	0.0505(50)	24.9(3.6)	23.9(1.4)			–1.287
			387.954	0.444(21)	219 (25)	273 (14)			–0.306
			395.338	0.0906(74)	44.7(6.0)	46.2(3.2)			–0.980
			407.176	0.0605(53)	29.8(4.1)	32.5(2.4)			–1.130

Table 3. (*continued*).

Upper level energy (cm^{-1})[a]	J	τ_k (ns)	Transition wavelength (nm)	Branching fraction	$g_u A_{ul}$ (10^6 s^{-1}) This work	DLSC[e]	XSCLQB[f]	MW[g]	$\log(g_i f_{ik})$ This work
			446.925	0.133(10)	65.7(8.6)	68.6(4.2)			–0.706
			517.678	0.0764(69)	37.7(5.3)	36.3(3.2)			–0.820
			554.868	0.0588(66)	29.0(4.5)				–0.873
			596.012	0.0257(69)	12.7(3.7)				–1.171
			646.346[d]	0.060(11)	29.6(6.3)				–0.731
			647.161[d]						
28418.965	8.5	7.15(12)[c]	406.108	0.472(20)	1189(55)	1440 (72)		799.2	0.469
			428.451	0.1029(80)	259 (21)	247(18)		153.0	–0.147
			445.639	0.0859(69)	216 (18)	187 (14)		115.2	–0.191
			486.481	0.0218(30)	54.9(7.6)	25.6(2.3)			–0.710
			519.261	0.181(13)	456(33)	457 (38)		298.8	0.265
			548.570	0.0971(81)	244 (21)	169 (18)		102.6	0.043
			586.503	0.0391(55)	98 (14)			23.4	–0.294
			626.433					3.6	
28540.957	7.5	27.7(3.8)[b]	385.166	0.218(18)	126(20)	145.6(8.0)			–0.553
			404.106	0.205(17)	118 (19)	121.6(6.4)			–0.537
			416.056	0.214(18)	124(20)	121.6(6.4)			–0.493
			426.223	0.0318(74)	18.4(4.9)				–1.300
			443.229	0.0383(85)	22.1(5.8)	19.4(1.4)			–1.186
			544.922	0.0825(99)	47.6(8.7)	45.3(4.6)			–0.673
			582.336	0.0586(99)	33.9(7.4)	21.3(3.7)			–0.764
			655.898	0.051(16)	29.3(10.1)				–0.723
			702.096	0.101(29)	58.3(18.6)				–0.365
28748.524	8.5	62.4(6.3)[b]	400.743	0.473(21)	136 (15)	163.8(9.0)			–0.483
			422.484	0.171(12)	49.3(6.1)	47.5(2.9)			–0.880
			439.187	0.0207(26)	5.98(96)	1.84(27)			–1.762
			478.803	0.0299(34)	8.6(1.3)				–1.527
			510.523	0.226(15)	65.1(7.9)	62.6(4.7)			–0.595
			538.826	0.0547(53)	15.8(2.2)	11.9(1.8)			–1.163
			575.999	0.0256(43)	7.4(1.4)				–1.435

Table 3. (*continued*).

Upper level energy (cm^{-1})[a]	J	τ_k (ns)	Transition wavelength (nm)	Branching fraction	$g_u A_{ul}$ (10^6 s^{-1}) This work	DLSC[e]	XSCLQB[f]	MW[g]	$\log(g_i f_{ik})$ This work
28856.898	7.5	12.4(1.0)[b]	380.534	0.242(16)	312 (33)	248 (14)		1110.4	–0.169
			399.010	0.408(21)	526 (50)	571 (30)		832.0	0.099
			410.656	0.0327(42)	42.1(6.4)	35.2(2.1)		108.8	–0.972
			420.558	0.1078(87)	139 (16)	106(6.4)		283.2	–0.433
			437.106	0.0133(36)	17.2(4.8)			22.4	–1.307
			476.330[d]	0.0101(41)	13.0(5.4)	10.2(1.3)			–1.353
			478.180[d]						
			479.550[d]						
			535.697	0.120(10)	155 (18)	120 (11)		294.4	–0.176
			571.812	0.0665(82)	86(13)	81.6(8.0)		139.2	–0.376
			642.578	w		31.4(4.3)			
29027.543	8.5	12.3(2)[b]	396.311	0.402(24)	589(36)	716 (36)			0.142
			417.560	0.128(10)	187 (15)	220(13)			–0.310
			433.869	0.160(12)	234 (19)	288 (18)			–0.179
			472.489	0.0099(23)	14.4(3.3)				–1.316
			503.351	0.0633(59)	92.6(8.7)	88.2(7.2)			–0.453
			530.843	0.0217(34)	31.8(5.0)				–0.871
			566.886	0.0710(69)	104(10)	100.8(9.0)			–0.300
			603.423	0.0543(68)	79.5(10.0)				–0.362
			678.896	0.0035(29)	5.1(4.3)				–1.450
			687.305	0.0106(74)	15.6(10.9)				–0.957
			752.900	0.023(14)	33.9(20.2)	45.0(7.2)			–0.540
			805.127	0.052(29)	75.8(41.8)				–0.133
29434.270	6.5	13.1(1.4)[b]	357.499	0.0168(33)	17.9(4.0)	192(11)	63.24		–0.349
			372.350	0.198(18)	211 (29)				
			379.147	0.0138(61)	14.7(6.7)	11.20(84)			–1.493
			390.022	0.550(24)	588(68)	553(28)	600.2		0.137
			426.343	0.0945(85)	101(14)	60.1(4.2)	101.0		–0.551

Table 3. (*concluded*).

Upper level energy (cm^{-1})[a]	J	τ_k (ns)	Transition wavelength (nm)	Branching fraction	$g_u A_{ul}$ (10^6 s^{-1}) This work	DLSC[e]	XSCLQB[f]	MW[g]	$\log(g_i f_{ik})$ This work
			540.617	0.0380(47)	40.6(6.7)	32.8(4.2)			–0.745
			553.532	0.0376(49)	40.2(6.8)	31.9(3.8)	30.25		–0.730
			574.127	0.0204(41)	21.8(5.0)	30.0(3.6)	30.84		–0.970
			584.632	0.0115(39)	12.3(4.4)		15.02		–1.211
			658.802	0.0191(77)	20.4(8.5)	19.6(4.2)	12.70		–0.895
29955.418	7.5	49.1(4.2)[c]	382.250	0.1070(84)	34.9(4.0)				–1.117
			392.926	0.288(17)	94.0(9.8)				–0.662
			401.981	0.213(14)	69.4(7.5)				–0.774
			417.074	0.0721(59)	23.5(2.8)				–1.212
			454.308	0.0460(56)	15.0(2.2)				–1.333
			455.545	0.0117(45)	3.8(1.5)				–1.927
			505.917	0.0418(47)	13.6(1.9)				–1.281
			538.008	0.0319(47)	10.4(1.8)				–1.345
			571.420	0.0218(51)	7.1(1.8)				–1.458
			600.199	0.0353(65)	11.5(2.3)				–1.207
			636.928	0.0362(85)	11.8(2.9)				–1.144
			642.166	0.0488(92)	15.9(3.3)				–1.007
			666.580	0.046(11)	14.9(3.7)				–1.002

[a]NIST Atomic Spectra Database [Ver. 3.0] available at http://physics.nist.gov/PhysRefData/ASD.
[b]Ref. 22.
[c]Ref. 23.
[d]Blended lines in this work.
[e]Ref. 21.
[f]Ref. 19.
[g]Ref. 14.
[*]This lifetime was incorrectly attributed to energy level 29 260.740 due to an error in the database of Ref. 17.

4. Results

As the first stage in the analysis, the results of our relative intensity measurements for radiative transitions in Nd II are presented in Table 2 since, unlike branching fractions, these data are unaffected by missing branches. For each upper level, the intensity of the strongest branch that we observed is set to 1. In Table 2, branches that we did not observe but are listed in earlier work are included in italics.

Table 3 presents our branching-fraction measurements, along with spontaneous-emission transition probabilities $g_u A_{ul}$ and $\log g_l f_{lu}$ values obtained by combining the branching fractions with our previously measured lifetime data [22, 23]. Transitions are identified by the upper-level energy, angular momentum J, and air wavelength, taken from the earlier references. The transition probabilities and the oscillator strengths were calculated using the well-known formulas for electric dipole transitions,

$$A_{ul} = \frac{R_{ul}}{\tau_u} \tag{3}$$

$$g_l f_{lu} = \frac{1}{0.66702\sigma_{ul}^2} g_u A_{ul} \tag{4}$$

where A_{ul} is the transition probability, R_{ul} is the branching fraction, τ_u is the upper-state lifetime, f_{lu} is the absorption oscillator strength, g_u and g_l are the $2J + 1$ statistical weights of the upper and lower levels, respectively, and σ_{ul} is the transition wave number (in cm^{-1}) [29].

Table 3 includes comparisons with the data of Den Hartog et al. [21], Xu et al. [19], and Maier and Whaling [14]. As a measure of agreement, we considered the difference in "units" of standard deviations, $\eta \equiv (gA_{\text{This work}} - gA_{\text{Other work}})/\sqrt{\sigma^2_{gA,\text{This work}} + \sigma^2_{gA,\text{Other work}}}$, which should have a mean of zero within error. For stronger transitions ($BF > 0.1$ or $g_u A_{ul} > 100 \times 10^6\ \mathrm{s}^{-1}$), the agreement of gA with other work is excellent, giving an average value $\bar{\eta} = -0.12(16)$. For weaker transitions, our gA values tend to be systematically larger, giving an average value $\bar{\eta} = 0.38(10)$, with the disagreement tending to become larger at longer wavelengths ($\lambda > 500$ nm). Saturation in our data as a possible cause can be ruled out experimentally. The correlation with line strength could arise from errors in the establishment of the baseline when spectral peaks are fit to determine their relative areas. Because of selective laser excitation, our spectra are simple and sparse, allowing the baseline to be easily set; our lock-in detection also greatly reduces any background, and in fact we observe the baseline to be quite flat. Spectra from discharge lamps are much more congested, which may lead to systematic errors in the extraction of areas of small peaks. A possible explanation for the correlation of the discrepancy with wavelength is a systematic error in the calibration of detection efficiency as a function of wavelength, since the Nd II spectral lines in the red region are generally weaker than those in the blue region of the spectrum.

5. Conclusions

We have measured 430 $\log gf$ values for Nd II transitions over the wavelength range 372–850 nm. These transitions originate from 46 upper levels in the range 22 697–29 955 cm^{-1}. The $\log gf$ values were obtained by combining measured relative intensities with previously measured radiative lifetimes. Highly selective laser excitation of only a single upper level produces a simple fluorescence spectrum, removing any ambiguity in the assignment of transitions to a pair of energy levels.

The error budget is dominated by systematic uncertainties in the efficiency calibration of the optical detection system, with smaller statistical contributions.

Acknowledgments

We are grateful to the Natural Sciences and Engineering Research Council of Canada for financial support.

References

1. G.M. Wahlgren. Phys. Scr. **T100**, 22 (2002).
2. E. Biémont and P. Quinet. Phys. Scr. **T105**, 38 (2003).
3. C.R. Cowley, T. Ryabchikova, F. Kupka, D.J. Bord, G. Mathys, and W.P. Bidelman. Mon. Not. R. Astron. Soc. **317**, 299 (2000).
4. S. Vauclair. Space Sci. Rev. **84**, 265 (1998).
5. J.J. Curry, E.A. Den Hartog, and J.E. Lawler. J. Opt. Soc. Am. B, **14**, 2788 (1997).
6. L. Dolk, G.M. Wahlgren, H. Lundberg, Z.S. Li, U. Litzén, S. Ivarsson, I. Ilyin, and S. Hubrig. Astron. Astrophys. **385**, 111 (2002)
7. L. Mashonkina, T. Ryabchikova, and A. Ryabtsev. Astron. Astrophys. **441**, 309 (2005)
8. L.S. Lyubimkov, T.M. Rachkovskaya, and S.I. Rostopchin. Astron. Rep. **40**, 802 (1996)
9. H.R. Butcher. Nature, **B328**, 127 (1987); C. Sneden, A. McWilliam, G.W. Preston, J.J. Cowan, D.L. Burris, and B.J. Armosky. Astrophys. J. **467**, 819 (1996).
10. J.E. Lawler, W. Whaling, and N. Grevesse. Nature, **346**, 635 (1990)
11. T. Ryabchikova, N. Piskunov, O. Kochukhov, V. Tsymbal, P. Mittermayer, and W.W. Weiss. Astron. Astrophys. **384**, 545 (2002)
12. W.F. Meggers, C.H. Corliss, and B.F. Scribner. NBS Monograph 145, Parts I and II. U.S. Government Printing Office, Washington, DC. 1975.
13. C.H. Corliss and W.R. Bozman. Monograph 53. U.S. National Bureau of Standards, Washington, DC. 1962.
14. R.S. Maier and W. Whaling. J. Quant. Spectrosc. Radiat. Trans. **18**, 501 (1977).
15. T. Andersen, O. Poulsen, T.S. Ramanujam, and A.P. Petkov. Sol. Phys. **44**, 257 (1975).
16. L. Ward, O. Vogel, A. Ahnesjö, A. Arnesen, R. Hallin, L. McIntyre, and C. Nordling. Phys. Scr. **29**, 551 (1984).
17. R.L. Kurucz and B. Bell. Atomic line data. Kurucz CD-ROM No. 23. Smithsonian Astrophysical Observatory, Cambridge, Mass. 1995.
18. http://cfa-www.harvard.edu/amdata/ampdata/kurucz23/sekur.html
19. H.L. Xu, S. Svanberg, R.D. Cowan, P.-H. Lefèbvre, P. Quinet, and E. Biémont. Mon. Not. R. Astron. Soc. **346**, 433 (2003).
20. http://w3.umh.ac.be/∼astro/dream.shtml
21. E.A. Den Hartog, J.E. Lawler, C. Sneden, and J.J. Cowan. Astrophys. J. Suppl. Ser. **148**, 543 (2003).
22. C.M. Pinciuc, R.C. Rivest, M.R. Izawa, R.A. Holt, S.D. Rosner, and T.J. Scholl. Can. J. Phys. **79**, 1159 (2001).
23. T.J. Scholl, R.A. Holt, D. Masterman, R.C. Rivest, S.D. Rosner, and A. Sharikova. Can. J. Phys. **80**, 713 (2002).
24. S.D. Rosner, D. Masterman, T.J. Scholl, and R.A. Holt. Can. J. Phys. **83**, 841 (2005).
25. S.J. Rehse, R. Li, T.J. Scholl, A. Sharikova, R. Chatelain, R.A. Holt, and S.D. Rosner. Can. J. Phys. **84**, 723 (2006).
26. J.L. Hall and S.A. Lee. Appl. Phys. Lett. **29**, 367 (1976).
27. L.H. Cadwell. Am. J. Phys. **64**, 917 (1996).
28. P.M. Koch, L.D. Gardner, and J.E. Bayfield. *In* Beam-foil spectroscopy. Vol. 2. *Edited by* I.A. Sellin and D.J. Pegg. Plenum, New York. 1976. p. 829.
29. W.C. Martin and W.L. Wiese. *In* Atomic, molecular, & optical physics handbook. *Edited by* G.W.F. Drake. AIP, New York. 1996.